Fluid-Structure Interaction in Civil Engineering Structures

Javier Rodríguez, María J. Crespo, Luis M. Lacoma, Francisco Martínez, and Joaquín Martí

Principia, Velázquez 94, 28006 Madrid, Spain

Abstract: The problems being addressed involve the dynamic interaction of solids (structure and foundation) with a liquid (water). Various numerical procedures are reviewed and employed to solve the problem of establishing the expected response of a structure subjected to seismic excitations while duly accounting for those interactions. The methodology is applied to the analysis of dams, lock gates, and large storage tanks, incorporating in some cases a comparison with the results produced by means of simplified analytical procedures.

Keywords: Seismic Effects, Coupled Analysis, Dams, Tanks, Lock Gates.

1. Introduction

The design of many civil engineering structures is often governed by the hydrodynamic loads exerted during earthquake excitation. Characteristic examples are dams, lock gates and large storage tanks.

The effects of the liquid are conveniently decomposed into an impulsive component (a liquid mass that behaves as if rigidly attached to the structure) and a convective component (corresponding to internal distortions of the liquid mass and its free surface).

The impulsive hydrodynamic pressure is traditionally taken into account by introducing added masses. The concept of added mass has been used for decades to design earthquake resistant gravity dams (Westergaard, 1933) and liquid storage tanks (Housner, 1954). The pressure distributions, and consequently the added masses, are obtained solving the Laplace partial differential equation. The main assumptions of these approaches are the incompressibility of the water and the infinite rigidity of the boundary conditions provided by the dam, reservoir or tank.

Over time those assumptions have been refined progressively to take account of the dam deformability, water compressibility, reservoir bottom absorption and dam-foundation interaction in earthquake excited dam-reservoir systems (Fenves and Chopra, 1985a, 1985b). In a similar fashion, for the case of liquid storage tanks, Veletsos and his coauthors have improved the hypotheses to include the flexibility of the container and soil interaction effects (Veletsos, 1984; Veletsos and Tang, 1990).

The above developments make it possible to introduce some improvements in seismic design methodologies, taking into consideration the aforementioned effects. The present work summarizes the results obtained using the Abaqus/Standard capabilities (SIMULIA, 2011) for three different types of structures: lock gates, gravity dams and large LNG (liquefied natural gas) storage tanks.

2. Methodology

Various approaches have been employed in the calculations that follow, including analytical approximations when possible. For numerical modeling with Abaqus (SIMULIA, 2011), acoustic elements have been used to model the fluid. The containment structure has been modeled either with structural elements, as in the case of the lock gate or the LNG tank, or with solid elements in the case of the gravity dams.

Momentum and energy must be transferred across the interface between the structural and acoustic elements. The pressure field generated by the acoustic elements creates a normal surface traction on the structure, and the acceleration field developed by the structural elements gives rise to pressures at the fluid boundary. The interface has been modeled with a surface-based coupling procedure. The results may be rather sensitive to the selection of master and slave surfaces: the master surface should be that with the higher impedance.

In the case of lock gates and gravity dams, the modal dynamics procedure is not applicable since it is necessary to implement radiating boundary conditions, which here have been introduced with acoustic infinite elements attached to the boundary.

The earthquake input has been prescribed directly at the base of the structure. However, in the case of the lock gates, appropriate impedances were specified under the liquid to represent its interaction with the ground and account for the energy radiated across that interface.

General steady state dynamics and time history analyses were performed in the frequency and time domains, respectively. The time history analyses in the case of the LNG tank were based on a modal dynamic procedure, while for the gravity dams and the lock gates full time domain integrations were performed.

3. Dams

3.1 Description of the dams

The dams studied here are two gravity dams dating from the sixties. Since a failure of these dams could lead to flooding of a nuclear power plant, the study of their seismic performance had to be conducted as part of the stress tests carried out for all nuclear reactors in Europe following the Fukushima accident in Japan. The dams can be seen in Figures 1 and 2: Dam A has a height of 40.5 m while Dam B reaches 64.8 m. The concrete is similar in both dams: Young's modulus is 30 GPa, Poisson's ratio is 0.2, compressive strength is 20 MPa, and tensile strength is 2 MPa.

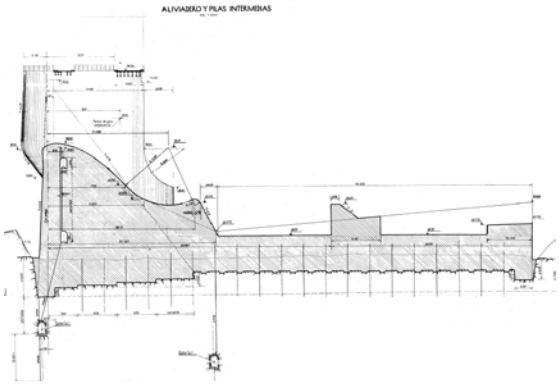

Figure 1 Section trough spillway Dam A

The ground at Dam B is essentially made of limestone, though some lignite layers could introduce potential weakness planes in the foundation. The intact rock was characterized with a Young's modulus of 22 GPa and a strength of 120 MPa. Perhaps more significantly, the lignite had a Young's modulus of 200 MPa, a cohesion of 70 kPa and a friction angle of 37º; the data came from large scale in-situ tests conducted in the lignite layers at the time of construction of the dam. The most likely sliding plane was assigned a friction coefficient of 0.8.

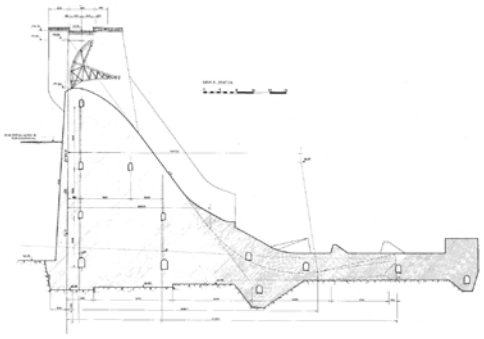

Figure 2 Section trough spillway Dam B

At Dam A the ground alternates sandstones and marls. There is little concern with the strength of the foundation, but the potential sliding of the dam is characterized with a friction coefficient of 0.7. Both at Dam A and at Dam B the contribution of the dam toe plays a significant role in relation with the sliding capacity; the estimated values are 5 MN/m in the case of Dam B and 2.5 MN/m in Dam A.

Pore pressure distributions underneath both dams were known from the installed piezometers and taken into account in assessing the stability.

3.2 Seismic input

The mandated seismic input for the dam is the one used for the seismic design of the plant. The design spectrum has a horizontal PGA (peak ground acceleration) of 0.13g and can be seen in Figure 3, the vertical spectrum was taken equal to 0.7 times the horizontal one.

To generate matching accelerograms, following the recommendations of ASCE 4-98 (ASCE, 2000), a 10 s duration was adopted. Three accelerograms were generated for the horizontal and vertical motions using SIMQKE (Gasparini, 1975) and POSTQUAKE (Woo, 1987). An example of one of the horizontal accelerograms is also shown in Figure 3.

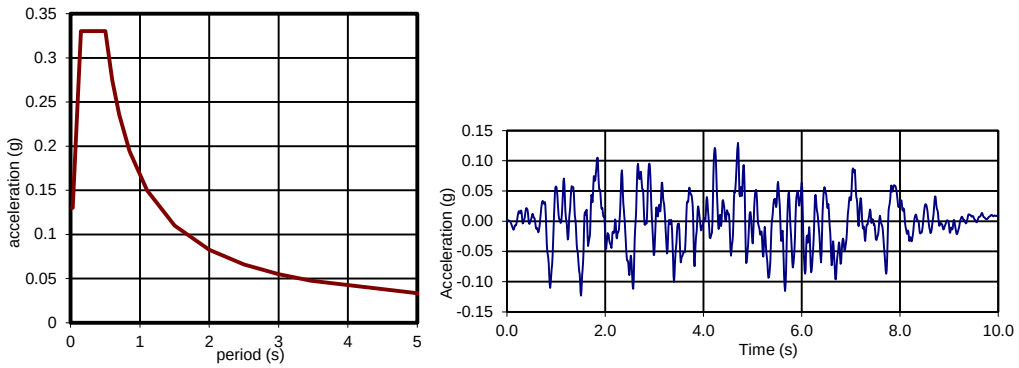

Figure 3 Design spectrum and horizontal accelerogram

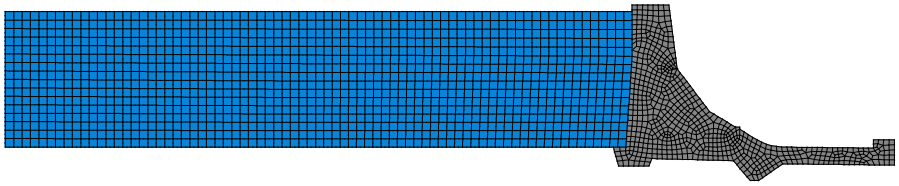

Figure 4 Finite element model for Dam B

3.3 Analysis and results

For Dam B, the analytical estimates afforded by the methodologies proposed by CFE (2008) and Bouaanani and his coworkers (2003, 2010) produce 5.8 Hz for the first frequency of the dam without water and 5.5 Hz for that of the reservoir. The proximity between these two frequencies already indicates that the compressibility of the water will play an important role in the response and that coupled analyses of the dam and the water are required.

The model used is shown in Figure 4, which combines plane strain elements for the body of the dam, plane stress elements with the appropriate width for the region of the spillway, and acoustic elements for the body of water. Frequency calculations with no acoustic elements yielded the first mode at 7.3 Hz, somewhat above the analytical estimate. A frequency sweep of the structural-acoustic model, using as input a harmonic excitation at the base, produced the maximum response amplification of the global system at 5.1 Hz.

The problem was then studied by direct time integration of the fully coupled system, using each of the three sets of accelerograms generated earlier. The results obtained were very similar with all three of them. The calculations allowed determining the evolution of horizontal and vertical forces acting on the dam, as required for an analysis of its stability; they also produced the stress states developed in the concrete to confirm its integrity.

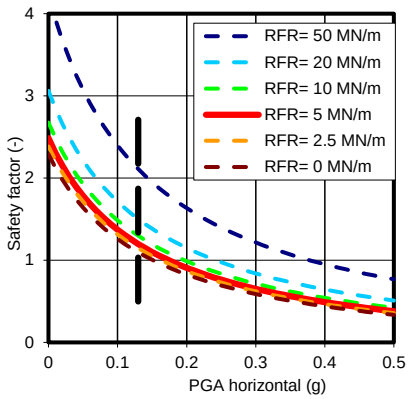

Figure 5 Dam B safety factor against sliding

Figure 5 indicates the safety factor against sliding as a function of the PGA and the toe capacity (RFR in the figure); the design conditions (PGA of 0.13g and RFR of 5 MN/m) are highlighted in the figure, which allows concluding that the safety factor is 1.20 and that sliding is only likely to occur with a PGA above 0.175g.

A similar procedure was followed for the Dam A. The analytical approaches again suggested that coupled analyses were necessary. The model generated for the dam appears in Figure 6, which again combines plane strain, plane stress and acoustic elements. The first frequency of the dam without water appears at 12.5 Hz and the harmonic frequency sweep indicates that the peak amplification of the global system takes place at 2.2 Hz.

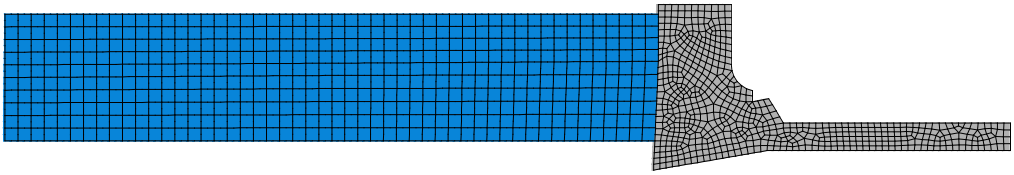

Figure 6 Finite element model for Dam A

Figure 7 indicates the safety factor against sliding as a function of the PGA and the toe capacity (RFR in the figure); the design conditions (PGA of 0.13g and RFR of 2.5 MN/m) are highlighted in the figure, which allows concluding that the safety factor is 1.08 and that sliding is only likely to occur with a PGA above 0.144g.

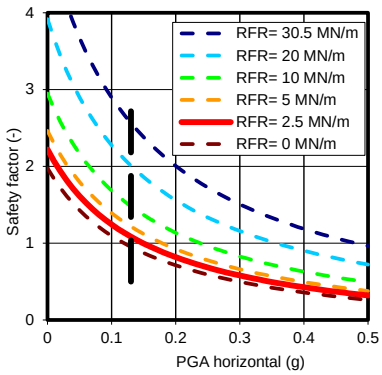

Figure 7 Dam A safety factor against sliding

4. Lock gates

4.1 Description of the gates

The locks analyzed here correspond to the so-called C-type locks to be placed in the current expansion of the Panama Canal. They are located in the Pacific side of the Canal, where the seismic hazard is considerably larger than towards the Atlantic end of the Canal. Only a summary description of the problem is provided here. All the data have been taken from the document prepared by UPC–CICP (2010), where additional details about the project can be found.

The dimensions of the lock gates are 57.600 x 32.645 x 10.000 m; they are made of steel and provide closure to a lock of 57.600 m width. The mass of the steel structure is 3800 t and it encloses 13,190 t of water. The water levels are 31.645 m upstream of the lock gate and 10 m downstream.

For the steel, the values of its mechanical characteristics will be a density of 7850 kg/m^3, a Young's modulus of 210 GPa and a Poisson's ratio of 0.3. For the water, the density will be taken as 1000 kg/m^3 and its bulk modulus as 2 GPa. The ground surrounding the lock gate is made of basalt rock, for which the density will be taken as 2650 kg/m^3 and the wave propagation velocity as 1737 m/s.

4.2 Seismic input

Prior studies by UPC–CICP (2010) had used artificial motions based on real earthquakes. However it appeared better to adopt motions that matched the provisions of applicable norms like ASCE 7 (ASCE, 2010). As a consequence, from the motions used in the study by UPC-CICP, the necessary parameters were obtained to allow constructing ASCE 7 spectra of the same size and it is the latter spectra that were used in the calculations. More specifically, to generate the spectrum for a 5% damping ratio, two spectral ordinates are needed; the values adopted were S_{DS} = 1.8g for

short periods and S_{D1} = 0.75g for 1 s period. The resulting spectrum, suitably modified for a damping ratio of 2.5%, which is considered realistic for the present structure, is shown in Figure 8.

As in the previous case, three sets of matching accelerograms were generated using SIMQKE and POSTQUAKE. The global duration adopted for the accelerograms was 25 s, which is a reasonable duration for the main motions of earthquakes of this size. An example appears in Figure 8.

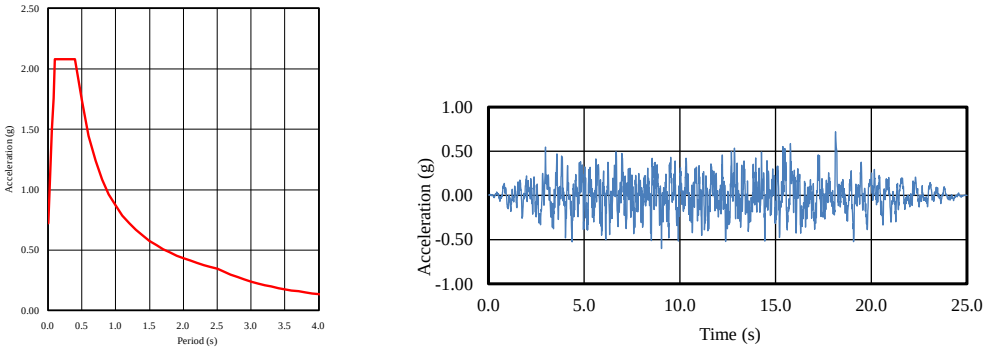

Figure 8 Design sprectrum and horizontal accelerogram

4.3 Analysis and results

The simpler and more traditional method was applied first. The effects of the water are introduced by means of added masses and the response spectrum procedure is used to determine the effects of the earthquake. In a subsequent implementation, the three-dimensional model used takes into account the flexibility of the gate, the compressibility of the water, and the radiation of energy through the ground.

The model developed, which can be seen in Figure 9, takes advantage of the longitudinal plane of symmetry; it includes the steel structure of the lock gate as well as the water contained in the lock. Displacements are assumed to be restrained along the part of its perimeter where the lock gate contacts the ground. The ground is characterized by means of its dynamic impedance.

The model allowed determining the first modes of vibration and their associated frequencies for the various elements of interest. Figure 10 presents the first natural mode of the lock gate by itself, without considering the water upstream or downstream from the gate, but incorporating the water inside the gate; the frequency of this first mode is 6.9 Hz.

A similar analysis yields 11.2 Hz for the first frequency of the water contained in the chamber behind the lock gate. When the lock gate and the water are analyzed together, the first mode of the joint system develops with a frequency of 2.8 Hz.

The pressures at the lock heel were determined for harmonic input as a function of its frequency. The results clearly peak at the frequency of 2.8 Hz, identified in the previous paragraph as the first frequency of the system. These results, normalized with the value of the hydrostatic pressure, are given in Figure 11. At resonance, when the input and natural frequencies coincide, the pressures in the water and those exerted on the lock gate are shown in Figure 12.

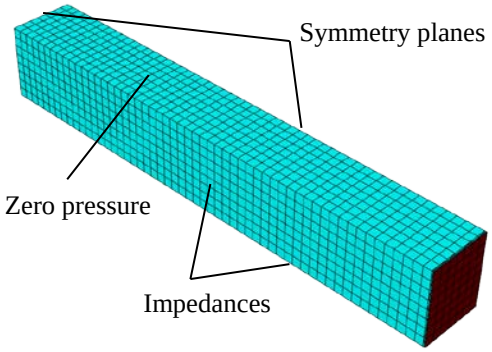

Figure 9 FE model

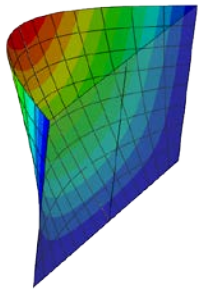

Figure 10 First mode of the lock gate (6.9 Hz)

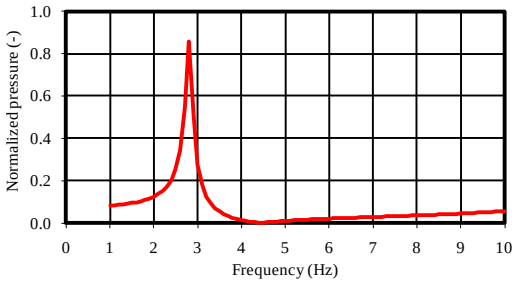

Figure 11 Normalised pressure at lock heel

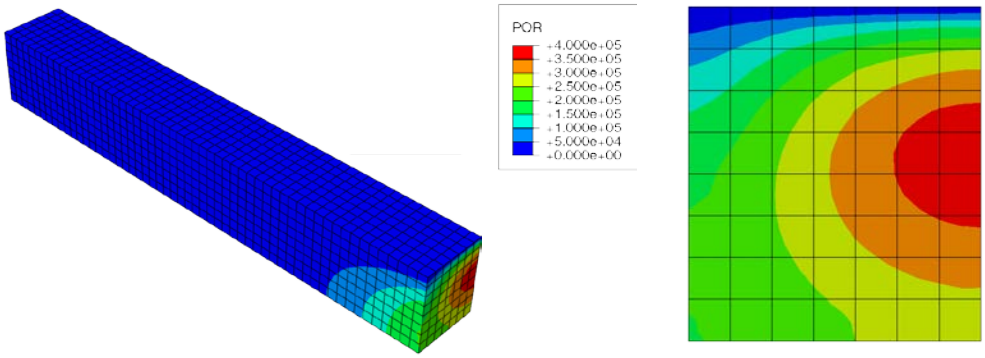

Figure 12 Pressures in the body of water and on the lock at resonance

The above results allow determining a distribution of added water masses for analysis of the lock gate as the ratio of the pressure and the acceleration. This distribution is presented in Figure 13. As an aside, it differs only marginally from that obtained when neglecting the compressibility of the water, the deformability of the gate and the radiation of energy through the ground.

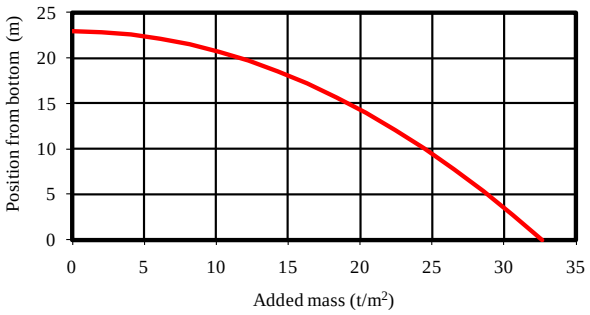

Figure 13 Added mass

A direct time integration of the fully coupled problem was then performed. The model is the same already presented earlier, which includes explicit representations of the water and the lock gate. The effects of the ground are introduced via the appropriate dynamic impedances. The calculations were repeated for each of the three accelerograms generated. The process simply consists in specifying that the ground follow the corresponding accelerograms and marching forward in time by direct integration of the equations governing the problem.

The calculations provide the maximum hydrodynamic pressures exerted on the lock gate. Figure 14 shows the peak pressures obtained for the three accelerograms used; they differ somewhat as a function of the specific accelerogram adopted, but the differences are minor. The maximum value of the hydrodynamic pressure developed at any point of the lock gate is about 0.4 MPa.

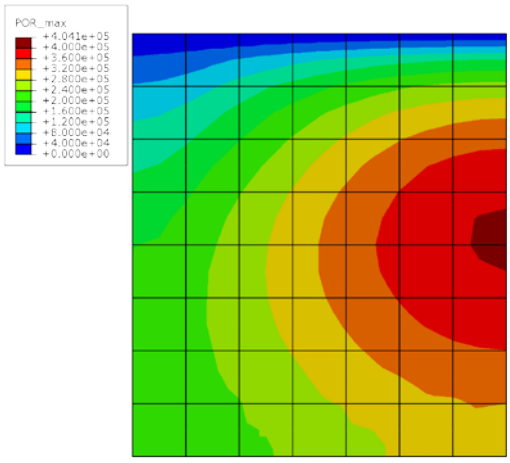

Figure 14 Pressures for earthquake 1

It is also worth mentioning that the presence of 10 m of water downstream from the lock gate has only minor effects on those pressure distributions, primarily because the water is located relatively near the perimeter of the gate. This conclusion was verified by placing 10 m of water downstream from the gate and repeating the analysis, which led to almost identical results.

Figure 15 compares the results obtained using the added mass procedure with those generated by direct integration of the fully coupled problem. The latter seems to give more favorable results in two senses: the peak pressures are smaller than those obtained on the basis of a response spectrum procedure with added masses, and the distribution of the hydrodynamic pressures is more even and therefore less harmful for the structural performance of the lock gate.

In summary, relaxing some of the traditional conservatisms (i.e.: going to three dimensions and accounting for the deformability of the gate, the compressibility of the water and energy radiated through the ground) had relatively minor effects on the results. In contrast, the solution procedure did seem to have a more important effect on the values of the pressures, as both the values of the peak pressures and their distribution on the gate appeared to be less structurally demanding on the lock gate when calculated by direct integration of the fully coupled problem.

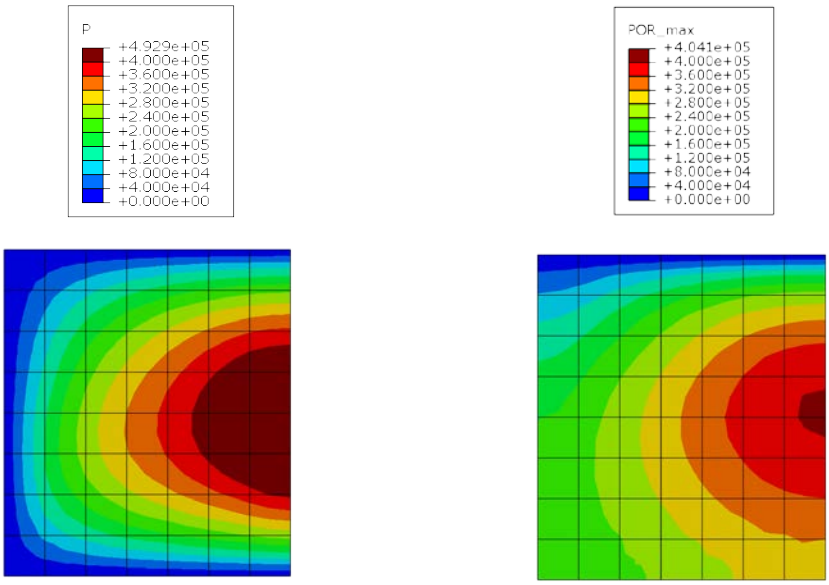

Added mass method

Coupled method

Figure 15 Pressures for both methods

5. LNG storage tanks

5.1 Description of the tank

LNG is normally stored in full containment, cylindrical tanks that actually consist of two tanks. The outer one is made of prestressed concrete and its basic purpose is to protect the contents against outside threats and to prevent leakage of the contents whether in liquid or vapor form. The inner one is a self-standing, open top tank made of cryogenic steel. The typical storage capacity of modern LNG tanks is 160,000 m^3. The storage temperature is -165ºC to ensure that methane remains in liquid form.

For the tank studied here, the inner tank has a radius of 40.00 m and in normal operation the liquid reaches an elevation of 33.65 m. The thickness of the inner tank decreases with elevation; the details will not be tabulated here, but the lower plates have a thickness of 24.4 mm and the thickness of the plates decreases with elevation to stabilize at 10.0 mm above 27.40 m.

The material of the inner tank is 9% Ni steel, with a Young's modulus of 200 GPa, Poisson's ratio of 0.3, and density of 7850 kg/m^3. At the storage temperatures, methane has a bulk modulus of 2.2 GPa and a density of 475 kg/m^3.

5.2 Seismic input

The mandated spectra for the SSE (safe shutdown earthquake) and OBE (operating basis earthquake) motions governing the design are shown in Figure 16.

To conduct time marching calculations it is necessary to generate accelerograms matching the design spectra. For the global duration and other characteristics of the earthquakes, the indications by GPEEEC (2007) were taken into account. The overall duration of the OBE was 32 s and that of the SSE was 36 s.

SIMQKE and POSTQUAKE were used again to generation 5 different accelerograms for each of the motions.

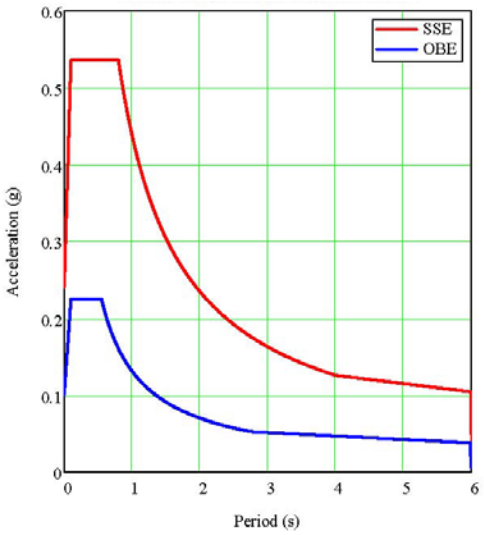

Figure 16 Design spectra for the LNG tank

5.3 Analysis procedure

To construct the finite element model, advantage was taken of the plane of symmetry presented by both the structure and the loading, which allows modeling only half of the structure.

The mesh used for representing the inner tank consists of approximately 2800 3D shell elements, which are shown in Figure 17, where the different colors identify the different shell thicknesses. The liquid was modeled by means of about 25,000 3D acoustic elements, as can be seen again in Figure 17.

As indicated in section 2 the interface between the inner side of the tank and the LNG is modeled with a surface based coupling, a coupling that generates automatically special elements provided with both mechanical and acoustic degrees of freedom (displacements and pressure). The mesh refinement in the structural and liquid parts of the model was carefully selected to ensure the correct performance of the connection between both and similar precautions were taken at the bottom interface.

The stiffeners of the inner tank were modeled using stringers, which basically consist in beam elements that share nodes with the underlying shell elements.

The hydrostatic pressure produced by the LNG at rest was applied first. The stress state generated in this fashion is taken as the base state for the subsequent calculation of the natural modes and frequencies and hence as the basis for the modal analysis process.

5.4 Results

An eigenvalue analysis was carried out first. The mode that mobilizes the largest mass in the longitudinal direction is the 9^{th} one, with a frequency of 2.00 Hz; Figure 18 shows how the inner tank deforms under this mode, which is indicative of the presence of the stiffeners.

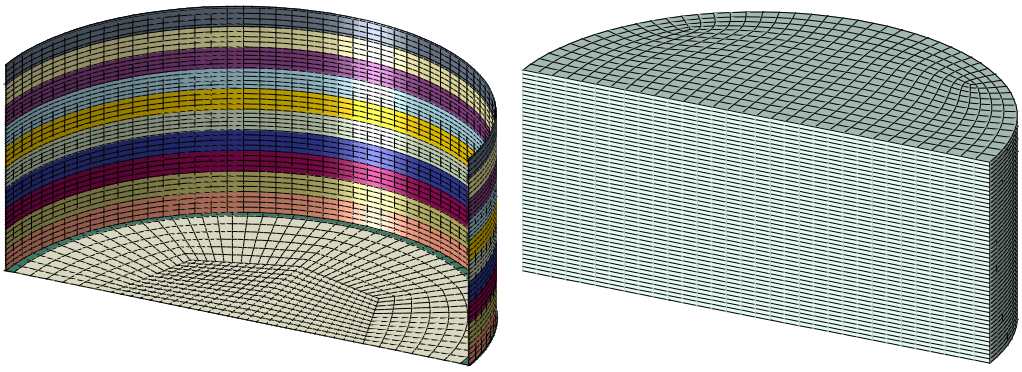

Figure 17 Meshes for the tank and the liquid

The equivalent mode, as derived in a previous study with a model that represented both the inner and outer tanks, had a frequency of 1.74 Hz. Analytical calculations based on Veletsos (1984) produced a fundamental frequency of 1.93 Hz. It can therefore be concluded that the present results are in good agreement with those generated with other methodologies.

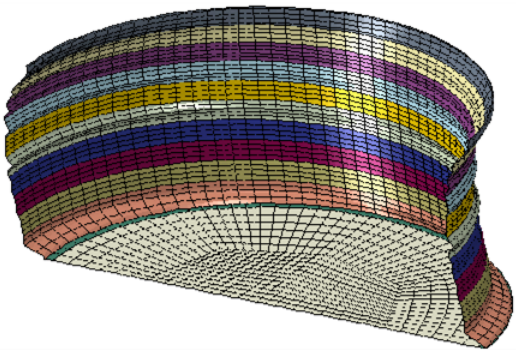

Figure 18 First eigenmode for the LNG tank

Of particular interest for the tank design are the section forces in the inner tank wall. Three different types of distributions of the section forces were retrieved from the calculations:

- Direct membrane forces in the vertical direction along the bottom perimeter.
- Direct membrane forces in the vertical direction along the most unfavourable generator in the wall.
- Direct membrane forces in the hoop direction along the most unfavourable generator in the wall.

The membrane forces in the vertical direction along the bottom wall perimeter are presented in Figure 19. The curves present the worst distribution generated when applying each of the five time histories. The theoretical distribution of the moment, as calculated using Veletsos' methodology, is also shown in the figure. Since Veletsos' results are derived using a response spectrum methodology, they must be taken to represent an upper bound. As can be seen, the finite element results are in good agreement with those produced with the analytical calculation by Veletsos.

Membrane forces along the least favorable generator are shown in Figures 20 and 21, the first one corresponds to OBE results, while the other is for SSE conditions. The first plot in Figure 20 shows distributions of individual membrane forces (vertical and hoop), corresponding both to the hydrostatic pressure conditions and to the seismic excitation; the latter reflects the worst distribution observed when applying each of the five time histories.

The hoop forces introduced by the seismic action are of the same order of magnitude but somewhat smaller than those induced by the LNG hydrostatic pressure. The vertical membrane forces remain small in comparison with the hoop direction. The allowable membrane force is also presented in this and subsequent figures.

The maximum allowable design stress for the steel in the OBE situation is 388 MPa, which is 1.33 times the allowable stress for service condition as per section 5.12.2 of EN 14620-2 (CEN, 2006). The second plot in Figure 20 presents the total membrane forces for OBE in the vertical and hoop directions. The combined membrane forces are between one half and two thirds of the maximum allowable values.

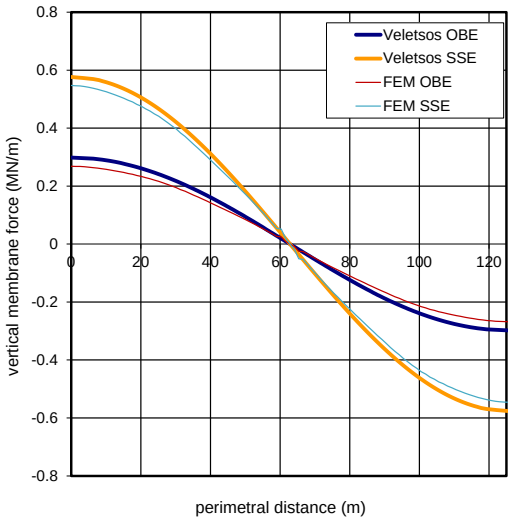

Figure 19 Membrane forces in the vertical direction of the LNG tank

Figure 21 is analogous to the previous one, except that it corresponds to the SSE situation. The allowable design stress for the steel is now the yield stress, namely 580 MPa. The observations are similar to the previous ones: the hoop forces introduced by the seismic action are still smaller than those induced by the hydrostatic pressure of the LNG at operating level and the vertical membrane forces remain negligible with respect to the hoop ones.

6. Conclusions

A number of problems have been addressed which involve the seismic response of civil structures in the presence of significant liquid-structure interaction effects. In particular, concrete dams, lock gates, and large LNG storage tanks have been studied. Methodologies range from rather conventional response spectra analyses using added masses, to the direct integration of the fully coupled problem. As a result of the studies presented, the following conclusions can be offered:

- The use of acoustic elements provides a relatively simple and reliable procedure for dealing with the dynamic liquid-structure interactions that arise during seismic excitation of structures such as dams, lock gates and storage tanks.
- More traditional procedures, such as the use of added masses and the response spectrum method, appear to provide reasonably accurate results, which can be refined by direct time integration of the fully coupled problem.

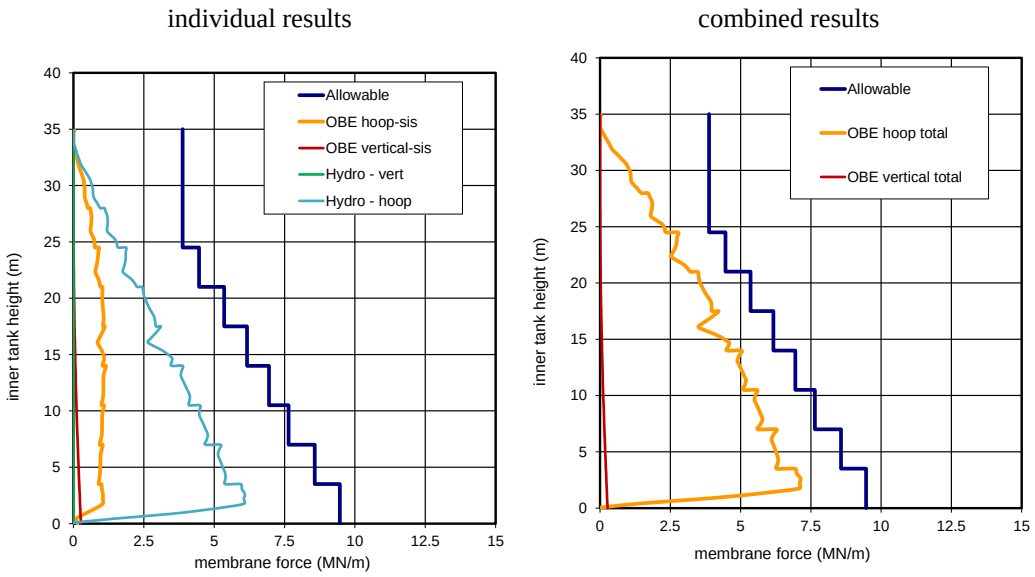

Figure 20 Membrane forces along the most unfavourable generator. OBE.

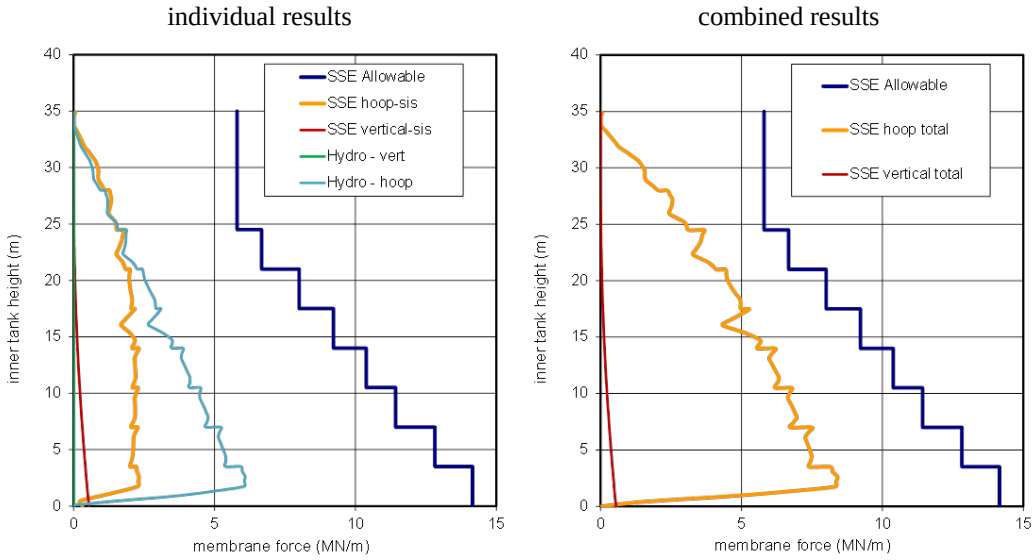

Figure 21 Membrane forces along the most unfavourable generator. SSE.

7. References

1. ASCE – American Society of Civil Engineers ((2000) "Standard 4-98. Seismic Analysis of Safety-Related Nuclear Structures and Commentary".
2. Bouaanani, N., Paultre, P., and Proulx, J. (2003) "A Closed-Form Formulation for Earthquake-Induced Hydrodynamic Pressure on Gravity Dams", Journal of Sound and Vibration, Vol. 261, pp. 573-582.
3. Bouaanani, N. and Perrault, C. (2010) "Practical Formulas for Frequency Domain Analysis of Earthquake-Induced Dam-Reservoir Interaction", ASCE Journal of Engineering Mechanics, Vol. 136, No. 1, January, pp. 107-119.
4. CEN – European Committee for Normalization (2006) "EN14620. Design and Manufacture of Site Built, Vertical, Cylindrical Flat-bottomed Steel Tanks for the Storage of Refrigerated, Liquefied Gases with Operating Temperatures between 0ºC and -165ºC. Part 2 Metallic Components", 20 February.
5. CFE – Comisión Federal de Electricidad (2008) "Manual de Diseño de Obras Civiles. Diseño por Sismo", Mexico, DF, December.
6. Fenves, A.M. and Chopra, A.K. (1985a) "Reservoir Bottom Absorption Effects in Earthquake Response on Concrete Gravity Dams", ASCE Journal of Structural Engineering, Vol. 111, No. 3, March.
7. Fenves, A.M. and Chopra, A.K. (1985b) "Simplified Earthquake Analysis of Concrete Gravity Dams: Combined Hydrodynamic and Foundation Interaction Effects", ASCE Journal of Engineering Mechanics, Vol. 111, No. 6, June.
8. Gasparini, D. (1975) "SIMQKE. A Program for Artificial Motion Generation", Department of Civil Engineering, Massachusetts Institute of Technology.
9. GPEEEC – Guandong Provincial Earthquake Engineering Experiment Center (2007) "Supplementary Report on Seismic Safety Evaluation on Guandong LNG Station Line Construction Site", December.
10. Housner, G.W. (1954) "Earthquake Pressures on Fluid Containers", California Institute of Technology.
11. SIMULIA (2011) "Abaqus Analysis User's Manual", Version 6.11, Providence, RI.
12. UPC–CICP (2010) "The Panama Canal. Third Set of Locks Project. Pacific Locks Complex. Lock Gates 3, 4, 5 & 6: Level 1 Seismic Analysis", Document No. P50/CICTCR-S1124, Rev. PB, 30 July.
13. Veletsos, A.S. (1984) "Seismic Response and Design of Liquid Storage Tanks", Guidelines for the Seismic Design of Oil and Gas Pipeline Systems, ASCE Technical Council on Lifeline Earthquake Engineering.
14. Veletsos, A.S. and Tang, Y. (1990) "Soil-Structure Interaction Effects for Laterally Excited Liquid Storage Tanks", Earthquake Engineering & Structural Dynamics, Vol. 19, Issue 4, May, pp. 473-496.
15. Westergaard, H.M. (1933) "Water Pressures on Dams during Earthquakes", Transactions of the ASCE, Vol. 98, pp. 418-433.
16. Woo, G. (1987) "POSTQUAKE. A Program to Generate Artificial Time Histories Matching Specified Seismic Response Spectra. User's Guide", Principia Mechanica Ltd.